EAI Endorsed Transactions
on Energy Web
Research Article EAI.EU

Research on flexible load configuration of hydrogen production and storage and operation optimization of distribution network based on bi-level optimization

Xuejie Wang[1,*], Changhao Song[1], Peng Ye[1], Tianyu Li[2], Zhiwei Xie[3], Shuo Yang[4], Jianming Qi[5], Yingxue Gao[5], Liang Dong[6]

[1]Shenyang Institute of Engineering, No. 18, Puchang Road, Shenbei New District, Shenyang City, Liaoning Province, China
[2]State Grid Jilin Electric Power Co., Ltd. Siping Power Supply Company, No. 999, Central West Road, Tiexi District, Siping City, China
[3]Hainan Nuclear Power Co., Ltd., No. 1, Nuclear Power Road, Changjiang Li Autonomous County, Hainan Province, P.R. China
[4]State Grid Liaoning Electric Power Co., Ltd. Fushun Power Supply Company, No. 1, Changcheng Street, Shengchan Zonghe Building & Measurement Center, Shuncheng District, Fushun City, Liaoning Province, P.R. China
[5]State Grid Liaoning Electric Power Co., Ltd. Benxi Power Supply Company, No. 21, Renmin Road, Pingshan District, Benxi City, Liaoning Province, P.R. China
[6]State Grid Liaoning Electric Power Co., Ltd. Shenyang Power Supply Company, No. 94, Bajing Street, Heping District, Shenyang City, Liaoning Province, P.R. China

Abstract

INTRODUCTION: High penetration of wind and photovoltaic generation causes voltage deviation, line congestion, and renewable curtailment in distribution networks. Hydrogen production and storage offer flexible regulation capabilities that can effectively improve system operational stability.
OBJECTIVES: This study aims to construct a bi-level optimization framework for capacity allocation and day-ahead scheduling in a wind–PV–hydrogen coupled system. The goal is to enhance voltage quality, reduce thermal loading, and increase renewable energy utilization.
METHODS: The upper level minimizes investment cost, network loss, and voltage deviation through a particle swarm optimization algorithm. The lower level solves a mixed-integer dynamic scheduling model in YALMIP considering grid trading cost, curtailment penalty, and peak-valley regulation benefits.
RESULTS: Simulation results show that the minimum node voltage rises from 0.913 p.u to 0.952 p.u, while the maximum line loading decreases from 0.903 to 0.714 after introducing hydrogen flexibility. The system load curve becomes smoother and renewable consumption significantly improves.
CONCLUSION: The proposed bi-level approach effectively enhances system flexibility and reduces operational constraints in distribution networks. The method offers practical support for coordinated planning of high-penetration renewable energy systems.

Keywords: Wind-solar hydrogen coupling, Distribution network, Bi-level optimization, Optimized scheduling

Received on 18 November 2025, accepted on 15 December 2025, published on 31 March 2026

Copyright © 2026 Xuejie Wang *et al.*, licensed to EAI. This is an open access article distributed under the terms of the CC BY-NC-SA 4.0, which permits copying, redistributing, remixing, transformation, and building upon the material in any medium so long as the original work is properly cited.

doi: 10.4108/ew.11918

1. Introduction

With the advancement of the strategic goal of carbon peaking and carbon neutrality, the installed capacity of distributed wind power and photovoltaic continues to grow [1], which

*Corresponding author. Email: 309195453@qq.com

makes the operation mode of distribution network show the characteristics of high fluctuation and high uncertainty [2]. When the wind and solar output is greater than the local load demand, it is easy to cause problems such as high node voltage, line overload and energy abandonment [3]. when the new energy output is insufficient, the peaking pressure of the system is increased [4]. Although the traditional load regulation and energy storage system can alleviate the fluctuation to a certain extent, its high cost and limited duration make it difficult to support long-term operation [5]. Hydrogen energy is regarded as a promising power-type flexible load in the power system because of its characteristics of producing hydrogen by electricity, storing energy by hydrogen, and using electricity again by hydrogen [6]. The hydrogen production and storage system can not only absorb excess electric energy (hydrogen production from electrolytic water) at low load, but also feed back to the power grid through fuel cell power generation at peak load [7]. It also has the functions of stabilizing power fluctuation, improving voltage quality and improving system elasticity [8].

In recent years, scholars have carried out a lot of research on the application of hydrogen energy systems in integrated energy networks. To improve the utilization of renewable energy, many studies have integrated hydrogen production and storage systems with wind power, photovoltaic generation, the power grid, and thermal energy systems. A multi-energy collaborative optimization model for electricity–hydrogen systems based on energy complementarity was proposed in [9,10]. By coordinating wind power hydrogen production and fuel cell power generation, energy balance at multiple time scales is achieved. In Niu M. et al. [11], an optimal scheduling model of electro-hydrogen system considering the dynamic response characteristics of electrolytic cell was constructed to reduce the operation cost under the premise of ensuring the stability of the system. The energy coupling between hydrogen storage tanks and hydrogen refueling stations was introduced in [12,13], and the integrated operation mechanism of wind and solar power, water electrolysis, hydrogen storage, and transportation was investigated, providing a new perspective for the application of hydrogen energy in the transportation sector.

In the distributed distribution network, the reasonable location and capacity configuration of hydrogen production and storage equipment have a significant impact on the economy and safety of the system. A method for siting and sizing hydrogen production systems based on an improved particle swarm optimization (PSO) algorithm was proposed in [14] and [15], in which minimum line loss and minimum voltage deviation are considered as dual optimization objectives. In [16], the bi-level programming model was used to realize the multi-regional optimal deployment of hydrogen production equipment in the distribution network, and its effectiveness in peak shaving and valley filling and reducing Wind and PV curtailment was verified. A multi-objective evolutionary algorithm was further proposed in [17], in which economic efficiency, reliability, and operational flexibility are considered to achieve the dynamic optimization of hydrogen production and storage in complex distribution network structures.

As a power-type flexible load, the hydrogen production and storage system can respond quickly under the fluctuation of electricity price index or grid frequency. A flexible adjustment unit was proposed by [18] to model the hydrogen production system, which aims to stabilize the fluctuation of wind and solar output. To address the problems of voltage violation and power flow congestion, an approach of realizing voltage support and line load balance through adaptive adjustment of flexible load was proposed by [19, 20]. The frequency stabilization effect of hydrogen energy load in the coordinated operation of multi-microgrid was studied by [21], and it was proved that its participation in primary frequency regulation can significantly improve the system stability. However, most of the current research still stays at the level of single-layer optimization or static configuration, and lacks dynamic optimization modeling of the coupling relationship between hydrogen production and storage system and distribution network operation.

To address voltage deviations, unbalanced power flows, line overloads, and challenges in consuming renewable energy caused by high penetration of wind and solar power, this paper proposes a two-layer optimization model of a wind-solar-hydrogen coupling system for distribution networks. The upper layer takes the capacity and access location of hydrogen production, hydrogen storage and fuel cell equipment as decision variables, and comprehensively considers the life cycle cost of equipment and the punishment of Wind and PV curtailment to realize the optimal planning of flexible load. The lower layer constructs a day-ahead operation optimization model based on YALMIP, and realizes the power balance and operation safety of the distribution network by coordinating the output of wind power, photovoltaic, hydrogen production, hydrogen storage and fuel cell. The main contributions of this paper include:

(i) It is proposed to embed the hydrogen energy flexible load as a regulating unit into the distribution network, and improve the system stability through the integrated optimization of capacity planning and operation scheduling.
(ii) A multi-dimensional operation evaluation system including voltage deviation, branch current carrying rate, network loss and peak-valley difference is established to realize the comprehensive analysis of different configuration schemes.
(iii) A hybrid solution framework of A global search is performed in the upper layer using PSO, while the lower layer employs YALMIP to obtain accurate solutions. is constructed to improve the adjustment ability of wind-solar-hydrogen coordinated operation. Based on the example verification of a 33-node distribution network, this method can significantly improve the voltage quality, reduce the line operating power and enhance the renewable energy consumption capacity.

2. Construction of wind-solar-hydrogen coupling system model in distribution network domain

The wind-solar-hydrogen coupling system is composed of wind power, photovoltaic, electrolytic hydrogen production equipment, hydrogen storage tank, fuel cell and distribution network. Each energy subsystem is coupled with each other through electric energy and hydrogen energy to realize coordinated scheduling of electric-hydrogen dual energy domain. This paper introduces the system structure, energy flow mechanism and the mathematical model of each equipment in detail, which lays the foundation for the establishment of the bi-level optimization model.

2.1. Distribution network operation framework with wind-solar hydrogen storage

The core idea of the wind-solar-hydrogen coupling system is to use hydrogen production and hydrogen storage as flexible loads to adjust the volatility of wind power and photovoltaic power generation. Through the main energy channels such as direct power supply of wind and solar, power supply to hydrogen production equipment and generation of hydrogen during low load periods, cross-period energy transfer by hydrogen storage tanks, feedback of fuel cells to distribution network by hydrogen power generation during peak hours, and purchase and sale exchange between distribution network and system, the system completes energy conversion and peak shaving under different load conditions, thereby reducing the intermittency and volatility of wind and solar power generation in the day.

2.2. Equivalent model of distributed power supply

The output power of photovoltaic solar panels will change with the influence of light intensity, air temperature and other factors. The simplified model of photovoltaic power station is [22]:

$$P_{\mathrm{PV}}(t)=P_{CT}\cdot(1+k(T(t)-T_{\mathrm{CT}}))\cdot\frac{B(t)}{B_{CT}} \tag{1}$$

In the formula: $P_{Pv}(t)$ is the output power of the photovoltaic power station at time t under the light intensity of $B(t)$; B_{CT} is the light intensity in the standard environment; T_{CT} is the air temperature in the standard environment; P_{CT} is the maximum output power of photovoltaic cells; k is the temperature coefficient; $T(t)$ is the surface temperature of the photovoltaic panel at time t.

When the wind speed is too low, the wind turbine speed is too slow to output power, and the wind speed at this time is called the cut-in wind speed. When the wind speed reaches the rated wind speed or higher, the wind turbine will output constant power. However, when the wind speed exceeds the critical value, in order to protect the wind turbine, the wind turbine will automatically turn off, and the wind speed at this time is called the cut-out wind speed [22].

$$P_{wind}=\begin{cases}0 & v>v_o, v<v_i\\ nP_{windN}\left(v^3-v_i^3\right)/\left(v_N^3-v_i^3\right) & v_i,\ v,\ v_N\\ nP_{windN} & v_N<v<v_o\end{cases} \tag{2}$$

In the formula: P_{wind} is the output of the wind turbine; v is wind speed; v_{i} is the cut-in wind speed of the wind turbine; v_{o} is the cut-out wind speed of the wind turbine; n is the number of wind turbines; P_{windN} is the rated output of wind power;

2.3. Equivalent model of hydrogen energy storage system

The mathematical model of the electrolytic cell is [23]:

$$\begin{cases}P_{Zh2N}=I_{Zh2}n_{Zh2}\left(U_{\mathrm{re}}+U_{\mathrm{pol}}+U_{\mathrm{ohm}}\right)\\ U_{\mathrm{ohm}}=\dfrac{z_1+z_2T_{Zh2}}{A_{Zh2}}I_{Zh2}\end{cases}. \tag{3}$$

In the formula: P_{Zh2} is the electric power consumption of the electrolytic cell; I_{Zh2} is the working current of the electrolytic cell; n_{Zh2} is the number of electrolytic cell series modules; U_{re} is the reversible voltage of the single electrolytic cell; U_{pol} is the polarization voltage of the single electrolytic cell; U_{ohm} is the ohmic voltage of the single cell; T_{Zh2} is the working temperature of the electrolytic cell; A_{Zh2} is the electrode area of the electrolytic cell; z_1 z_2 is the ohmic parameter of the electrolyte.

The mathematical model of the electrolytic cell is expressed as [24]:

$$\begin{cases}V_{Zh2N}=\dfrac{n_{Zh2}I_{Zh2}}{2F}\eta_{\mathrm{F}}\\ \eta_{\mathrm{F}}=96.5\exp\left(\dfrac{0.09}{I_{Zh2}}-\dfrac{75.5}{I_{Zh2}^2}\right)\end{cases} \tag{4}$$

In the formula: V_{Zh2N} is the hydrogen production rate of the electrolytic cell; η_{F} is Faraday efficiency F is Faraday constant.

The high-pressure gas tank is used to store hydrogen. It is assumed that the gas tank is a non-destructive closed system. According to the Clapeyron equation, the mathematical model of the hydrogen storage device is [24]:

$$\begin{cases} Q(t+\Delta t)=\int_{t_0}^{t_0+\Delta t} q(t)\mathrm{d}t+Q(t) \\ p(t)Q_Z=n(t)RT \end{cases} \tag{5}$$

In the formula: $Q(t_0+\Delta t)$ is the volume of hydrogen at time $(t_0+\Delta t)$; $q(t)$ is the hydrogen storage rate at time t; $Q(t)$ is the volume of hydrogen at time t; $p(t)$ is the pressure value of the hydrogen storage tank at time t; Q_Z is the total volume of the hydrogen storage tank; $n(t)$ is the molar amount of hydrogen at time t; R is a gas constant; T is the thermodynamic temperature of gas.

The mathematical model of fuel cell is expressed as [25]:

$$\begin{cases} P_{pceil}=U_{pceil}I_{pceil} \\ U_{pceil}=n_{pceil}(E_{\mathrm{n}}-U_{\mathrm{act}}-U_{\mathrm{ohm},pceil}-U_{\mathrm{con}}) \end{cases} \tag{6}$$

$$\begin{cases} E_{\mathrm{n}}=1.229-a(T_{pceil}-298.15\mathrm{K})+ \\ bT_{pceil}\left(\ln P_1+\frac{1}{2}\ln P_2\right) \\ U_{\mathrm{act}}=-(\varepsilon_1+\varepsilon_2T_{pceil}+\varepsilon_3T_{pceil}\ln C_2+\varepsilon_4T_{pceil}\ln I_{pceil}) \\ U_{\mathrm{ohm},pceil}=I_{fc}\left(R_{\mathrm{C}}+\frac{\rho_{\mathrm{M}}l}{A_{fc}}\right) \\ U_{\mathrm{con}}=m\exp\left(ni_{pceil}\right) \end{cases} \tag{7}$$

In the formula: P_{pceil} is the output power of the fuel cell; U_{pceil} is the output voltage of fuel cell; I_{pceil} is the working current of fuel cell; n_{pceil} is the number of single cell series; E_{n} is the thermodynamic electromotive force of single cell; U_{act} is the activated polarization overvoltage; $U_{\mathrm{ohm},pceil}$ is the fuel cell ohmic polarization overvoltage; U_{con} is the concentration polarization overvoltage; both a and b are constants; T_{pceil} is the working temperature of the stack; ε_1 to ε_4 is the activation coefficient; P_1 and P_2 are the effective partial pressures of hydrogen and oxygen at the interface between catalyst and gas, respectively. C_2 is the dissolved concentration of oxygen at the gas-liquid interface; R_{C} is the equivalent resistance of the electron flow channel; l is the thickness of the membrane; A_{pceil} is the activation area of the membrane; m and n is the concentration overpotential coefficient; I_{pceil} is the current density; ρ_{M} is the resistivity of the proton exchange membrane, the expression is:

$$\rho_{\mathrm{M}}=\frac{181.6\left[1+0.003i_{pceil}+0.062(T_{pceil}/330K)^2i_{pceil}^{2.5}\right]}{(\lambda-0.634-3i_{pceil})\exp\left(4.18\frac{T_{pceil}-303K}{T_{pceil}}\right)} \tag{8}$$

In the formula: λ is the water content of proton exchange membrane.

The expression of hydrogen consumption rate v_{pceil} of fuel cell is:

$$v_{pceil}=\frac{n_{pceil}I_{pceil}}{2F} \tag{9}$$

In the formula: F is the Faraday constant.

3. Wind-solar hydrogen storage bi-level optimization model

In order to realize the coordinated optimization operation of the wind-solar-hydrogen coupling system in the distribution network, this chapter constructs a two-layer optimization framework composed of the upper layer model of capacity planning and the lower layer model of operation scheduling. The upper model takes the minimum investment and configuration cost as the goal, and the lower model takes the system operation cost and operation stability as the goal. The mutual coupling between the two layers is realized by power balance equation, output constraint and power flow constraint.

3.1. Upper optimization model

The upper model takes the whole life cycle of the system as the starting point, and establishes the minimum annual average cost model f_1 of the whole life cycle as the goal, including the cost of wind and solar generating units B_{CPW}, the cost of energy storage devices B_{CC}, the cost of abandoning wind and solar B_{C_dg}, the cost of purchasing electricity B_{Cbuy}, the cost of selling electricity B_{Csell}, and the profit of selling hydrogen B_{CEh2}.

$$\min f_1=B_{CPW}+B_{CC}+B_{C\_dg}+B_{Cbuy}-B_{csell}-B_{CEh2} \tag{10}$$

The initial input cost of the system covers equipment procurement, engineering construction, on-site installation and commissioning adaptation and other related expenditures; the cost of operation and maintenance and fault handling refers to the various costs generated in the process of daily operation and maintenance support and fault investigation and repair after the equipment is officially put into use; the cost of asset disposal refers to the related expenditure generated by scrap processing, residual value recovery and other links when the equipment reaches the service life.

The mathematical model of wind power photovoltaic cost is expressed as:

$$B_{CPW}=B_{CPv}+B_{CPw} \tag{11}$$

$$B_{CPv}=\frac{C_{Pv\_d}P_{PvN}}{N}+\frac{\beta_1C_{Pv\_OM}P_{PvN}}{\beta_2}+\frac{C_{Pv\_S}P_{PvN}}{\beta_3} \tag{12}$$

$$B_{CWind}=\frac{C_{Wind\_d}P_{WindN}}{N}+\frac{\beta_1C_{Wind\_OM}P_{WindN}}{\beta_2}+\frac{C_{Wind\_S}P_{WindN}}{\beta_3} \tag{13}$$

In the formula: B_{CPv} is the cost of photovoltaic device; B_{CWind} are the cost of wind power device; in the calculation, the fault cost and operation and maintenance cost are merged into the operation and maintenance cost; C_{Pv_d} C_{Pv_OM} C_{Pv_S} are the unit capacity construction cost, operation and maintenance cost and disposal cost of the photovoltaic device; C_{Wind_d} C_{Wind_OM} C_{Wind_S} are the unit capacity construction cost, operation and maintenance cost and disposal cost of the wind power device; β_1 β_2 β_3 are the annual interest rate coefficients of construction cost, operation and maintenance cost and disposal cost respectively.

The mathematical model expression of energy storage device cost is:

$$B_{CC} = B_{CH2} + B_{CS} + B_{Cb} \tag{14}$$

$$B_{CH2} = \frac{C_{H2\_d}P_{H2N}}{N} + \frac{\beta_1 C_{H2\_OM}P_{H2N}}{\beta_2} + \frac{C_{H2\_S}P_{H2N}}{\beta_3} \tag{15}$$

$$B_{CS} = \frac{C_{CS\_d}P_{CSN}}{N} + \frac{\beta_1 C_{CS\_OM}P_{CSN}}{\beta_2} + \frac{C_{CS\_S}P_{CSN}}{\beta_3} \tag{16}$$

$$B_{Cb} = \frac{C_{b\_d}P_{bN}}{N} + \frac{\beta_1 C_{b\_OM}P_{bN}}{\beta_2} + \frac{C_{b\_S}P_{bN}}{\beta_3} \tag{17}$$

In the formula: B_{CH2} B_{CS} B_{Cb} is the cost of hydrogen production device, hydrogen storage device and fuel cell respectively; C_{H2_d} C_{H2_OM} C_{H2_S} are the unit capacity construction cost, operation and maintenance cost and disposal cost of the hydrogen production device; C_{CS_d} C_{CS_OM} C_{CS_S} are the unit capacity construction cost, operation and maintenance cost and disposal cost of the hydrogen storage device; C_{b_d} C_{b_OM} C_{b_S} are the unit capacity construction cost, operation and maintenance cost and disposal cost of the fuel cell device; N is the service life of the equipment.

Due to the instability and uncertainty of the wind and solar, it is inevitable to cause energy waste such as Wind and PV curtailment during the operation of the system.

The mathematical model expression of Wind and PV curtailment cost is:

$$\begin{aligned} B_{C\_dg} &= \sum \alpha_{\mathrm{CR}} P_{\mathrm{CR}} \\ P_{\mathrm{CR}} &= P_{\mathrm{wind}}^{\mathrm{cr}} + P_{\mathrm{PV}}^{\mathrm{cr}} \end{aligned} \tag{18}$$

In the formula: B_{C_dg} is the power of Wind and PV curtailment; α_{CR} is the penalty coefficient of power abandonment; $P_{\mathrm{wind}}^{\mathrm{cr}}$ $P_{\mathrm{PV}}^{\mathrm{cr}}$ is the abandoned wind power and abandoned solar power.

The actual output constraint of wind and solar:

$$0 \le P_{wind\_shiji}(t) \le P_{wind\_yuce}(t) \tag{19}$$

$$0 \le P_{pv\_shiji}(t) \le P_{pv\_yuce}(t) \tag{20}$$

The mathematical model expression of power purchase cost is:

$$B_{Cbuy} = P_{Cbuy}R_b \tag{21}$$

In the formula: B_{Cbuy} is the cost of purchasing electricity; R_s is the Power purchase price.

The mathematical model expression of electricity selling cost is:

$$B_{Csell} = P_{\mathrm{wind\_grid}}R_{\mathrm{wind}} + P_{\mathrm{pv\_grid}}R_{\mathrm{pv}} + P_{\mathrm{b\_grid}}R_s \tag{22}$$

In the formula: B_{Csell} is the cost of electricity sales, $P_{\mathrm{wind\_grid}}$ $P_{\mathrm{pv\_grid}}$ $P_{\mathrm{b\_grid}}$ is the cumulative on-grid power of wind power, photovoltaic and fuel cell respectively; R_{wind} R_{pv} R_s are the on-grid price of wind power, photovoltaic, fuel cell;

The mathematical model of hydrogen sales revenue is expressed as:

$$B_{CEh2} = Q_{\mathrm{H_2}}R_{\mathrm{H_2}} \tag{23}$$

In the formula: B_{CEh2} for the sale of hydrogen income; $Q_{\mathrm{H_2}}$ is the volume of hydrogen sold; $R_{\mathrm{H_2}}$ is the price of hydrogen sold.

3.2. Lower level optimization model

The lower model aims at minimizing the system operating cost and operating risk, and realizes the mutual coupling between the two layers through energy balance equation, equipment constraints and power flow constraints. Based on the given upper-level decision variables, YALMIP is used to solve the day-ahead operation optimization problem. The system operation cost is minimized through the optimization of equipment start-stop, energy flow distribution and power purchase and sale strategy. The energy balance equation, equipment constraints and power flow constraints are used to realize the mutual coupling between the two layers.

Operation constraints of hydrogen production system

$$0 \le P_{Zh2}(t) \le P_{Zh2N} \tag{24}$$

In the formula: $P_{Zh2}(t)$ is the hydrogen production power at t times, and P_{Zh2N} is the rated hydrogen production power of the electrolytic cell.

Hydrogen storage system operation constraints:

$$C_{h2}(t) = C_{h2}(t-1) + C_{h2\_in}(t) - C_{h2\_out}(t) \tag{25}$$

$$0 \le C_{h2}(t) \le C_{ccsN} \tag{26}$$

$$C_{h2}(1) = C_{h20} = 50 \tag{27}$$

$$C_{h20} \le C_{h2}(24) \le C_{ccsN} \tag{28}$$

In the formula: $C_{h2}(t)$ is the hydrogen storage capacity of the system at t times; $C_{h2}(t-1)$ is the hydrogen storage capacity of the system at $t-1$ moments; $C_{h2\_in}(t)$ is the amount of hydrogen; $C_{h2\_out}(t)$ is the amount of hydrogen; C_{h20} is the initial reserves; C_{ccsN} hydrogen storage equipment capacity; the reserves shall not be less than zero at any time, and shall not exceed the capacity of hydrogen storage equipment C_{ccsN}. It is also required that the reserves should be kept within the feasible range at the end of the scheduling to ensure that the operation on the next day is still feasible.

Fuel cell operation constraints:

$$0 \le P_{pceil}(t) \le T_{emp\_ceil}(t) \cdot P_{ceilN} \tag{29}$$

$$C_{h2\_waste}(t) + C_{pceil}(t) = C_{h2\_out}(t) \tag{30}$$

In the formula: $P_{pceil}(t)$ is the output power of the fuel cell; P_{ceilN} is the rated output power of fuel cell; $T_{emp\_ceil}(t)$ is the start-stop state, and $T_{emp\_ceil}(t)$ is the binary decision variable. When the value is 1, it means that the operation is allowed, and when the value is 0, it means that the operation is stopped. $C_{pceil}(t)$ is the actual hydrogen consumption; $C_{h2\_waste}(t)$ is the amount of hydrogen abandoned; the hydrogen required for the operation of the fuel cell is provided by the hydrogen storage tank 's hydrogen output $C_{h2\_out}(t)$, which includes the actual consumption of hydrogen $C_{pceil}(t)$ and the amount of hydrogen discarded $C_{h2\_waste}(t)$, ensuring that the energy source of the fuel cell is consistent with the hydrogen storage system.

The voltage quality is measured by the voltage deviation, which is defined as the sum of squared deviations between each node voltage and the reference voltage. The mathematical expression is as follows:

$$VD(t) = \sum_{i=1}^{n} \frac{(U_i(t)-1)^2}{1.05-0.95} \tag{31}$$

In the formula: $VD(t)$ is the voltage deviation index of time t, $U_i(t)$ is the voltage amplitude of the i node at time t, which measures the square deviation of the voltage of the whole network node relative to 1 $p.u$ and normalizes it to the allowable range.

In order to describe the overall operation effect of the wind-solar-hydrogen coupling system in the distribution network, a comprehensive operation index function is constructed to quantify the comprehensive impact of the system on the distribution network. The index consists of two parts, one part reflects the level of network loss caused by system operation, and the other part reflects the influence of voltage deviation on power quality. The mathematical expression of the index is:

$$J_{\text{comp}} = \sum \alpha\, ploss(t) + \sum \beta \sqrt{VD(t)/24} \tag{32}$$

In the formula: J_{comp} is the comprehensive operation index, $ploss(t)$ is the active power loss caused by the system operation at t time points, which can reflect the influence of power flow distribution and equipment configuration on transmission loss; α β serves as the weighting factor, used to balance the importance of network losses and voltage quality.

In the power flow calculation of distribution network, in order to ensure the safety of line operation, it is necessary to monitor whether the actual current of each branch exceeds its rated capacity. To this end, the line overload index is introduced:

$$\Phi_{OS}(t) = \left[\max(0, I_l^{rated}(t) - I_l^{act}(t))\right] \tag{33}$$

In the formula: $\Phi_{OS}(t)$ denotes the line safety margin value at time t; $I_l^{act}(t)$ denotes the branch rated current at time t; $I_l^{rated}(t)$ denotes the actual branch current in the power flow at time t; This function measures the relative deviation of branch current from the rated upper limit. When the actual branch current falls below the rated current, this term is zero; when the actual current exceeds the rated value, this term increases proportionally to the magnitude of the deviation. Consequently, $\Phi_{OS}(t)$ reflects the impact of operational schemes on line safety margins, providing upper-level optimisation with overlimit constraints or penalty information to guide the rational configuration and deployment of hydrogen production loads and distributed power sources.

The branch line loading rate measures the ratio of the power flow of the branch to its rated power. In order to ensure the safe operation of the system, the branch line loading rate should not be too high. The line loading rate can be calculated by the following formula:

$$LR(t) = \frac{I_l^{rated}(t)}{I_l^{act}(t)} \tag{34}$$

In the formula: $LR(t)$ is the line loading rate at time t; when the branch line loading rate exceeds 0.8 or below 0.4, the penalty is included:

Power flow balance equation:

$$\begin{aligned} P_i &= V_i \sum_{j \in N} V_j \left(G_{ij}\cos\theta_{ij} + B_{ij}\sin\theta_{ij}\right) \\ Q_i &= V_i \sum_{j \in N} V_j \left(G_{ij}\sin\theta_{ij} - B_{ij}\cos\theta_{ij}\right) \end{aligned} \tag{35}$$

And meet:

$$\begin{aligned} P_i + P_{load,i} &= P_{inj,i} \\ Q_i + Q_{load,i} &= Q_{inj,i} \end{aligned} \tag{36}$$

In the formula: P_i node i distributed energy or load active power injection; the active load of $P_{load,i}$ nodes and i places; $P_{inj,i}$ node i is injected into the total active power of the grid; Q_i nodes and i active power injection of distributed energy or load; the active load of $Q_{load,i}$ nodes and i places; $Q_{inj,i}$ nodes i are injected into the total active power of the grid.

3.3. Bi-level optimization solution idea

In the upper optimization, the power of hydrogen production equipment P_{Zh2N}, the capacity of fuel cell P_{ceilN}, the capacity of hydrogen storage device C_{ccsN} and the location of its access node L_c are used as decision variables to form the position vector of the individual particle swarm. The particle swarm optimization algorithm uses randomly initialized multiple groups of particles as candidate solutions, and achieves global optimization through speed update and position iteration. In each iteration, the particle swarm updates the device capacities and access schemes according to the synergy between the historical best position and the individual best position. This process aims to improve the upper-level objective function, including comprehensive network loss, voltage deviation, load balance, and other performance indicators.

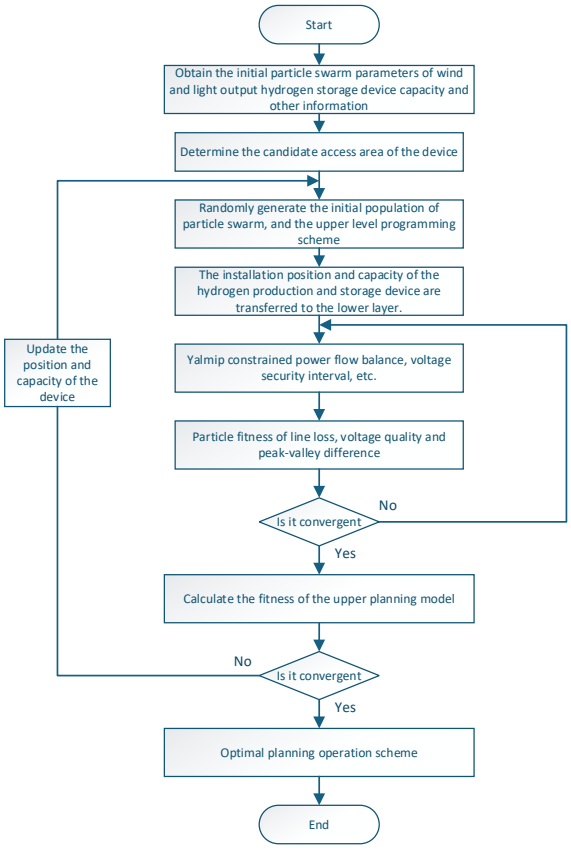

Figure 1. Flow chart of bi-level optimization model

Secondly, for each candidate scheme generated by PSO, the lower-level distribution network operation optimization model based on YALMIP is called to solve. The lower model takes the given capacity and access node as input, and calculates the optimal operation mode of the system within 24 hours by establishing multi-dimensional constraints such as wind and solar output, hydrogen production power, fuel cell output, hydrogen storage state, voltage constraint and branch power flow constraint. YALMIP invokes the built-in solver to solve the hourly power distribution, and the output includes hydrogen storage curve, hydrogen production and hydrogen release power, branch power flow, node voltage and other operating quantities. The running results will be input into the upper PSO as a fitness function to evaluate the pros and cons of the current particles.

Thirdly, the comprehensive operation index, including system network loss, branch over-limit risk, voltage deviation, and peak-valley difference improvement, is computed by the upper-level PSO based on the results of the lower-level operation and used to update the optimal candidate scheme. If the particle swarm does not meet the termination condition, then continue to iterate; if the maximum number of iterations or the global optimal solution is stable, the final capacity configuration and access location scheme are output. Figure 1 shows the flow chart of the bi-level optimization model.

4. Examples and results points

4.1. Simulation platform and parameter setting

To validate the proposed bi-level optimization method for the wind-solar-hydrogen coupling system, this paper develops a simulation platform consisting of upper-layer capacity configuration, lower-layer day-ahead scheduling, and distribution network power flow calculation. The simulation procedure is summarized as follows:

In the upper part, the particle swarm optimization algorithm PSO is used to optimize the configuration of hydrogen production power P_{Zh2N}, fuel cell power P_{pceilN}, hydrogen storage tank capacity C_{ccsN} and access node L_c. The upper optimization results are transmitted to the lower scheduling module through the parameter vector.

The lower part uses YALMIP to call the solver. Based on the given wind power prediction scenario, photovoltaic prediction scenario, load data and optimized equipment capacity, the actual output of wind and solar power P_{wind_shiji} and P_{pv_shiji}, electrolytic cell hydrogen production power P_{Zh2}, fuel cell power P_{pceil}, hydrogen storage capacity C_{h2} variables are solved respectively. Finally, the voltage qualification and network loss level are verified by power flow calculation.

The whole simulation process is run on the MATLAB R2022b platform. The optimization and power flow calculation are completed in the same environment. The rated

power of hydrogen production is 800 kW, the hydrogen storage capacity is 2400m^3, and the rated power of fuel cell is 1200 kW. The total load data of the system are taken from the typical daily load curve. Figure 2 depicts the self-constructed 33-node distribution network model, in which node 1 is designated as the slack bus. According to the power flow distribution characteristics and load density of the system, the whole network is divided into four candidate hydrogen production and storage access areas:

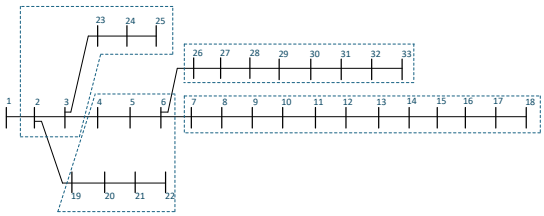

Figure 2. 33 node model candidate region diagram

The nodes in each region are comprehensively evaluated according to voltage margin, line current carrying rate and load density as potential access points for hydrogen production and storage systems. The PSO algorithm is used to optimize the capacity vectors of four types of hydrogen production and storage units in continuous space:

$$\mathbf{x} = [C_{Zh2N,1\sim4}, C_{PceilN,1\sim4}, C_{ccsN,1\sim4}, L_{c,1\sim4}] \tag{37}$$

Among them: $C_{Zh2N,1\sim4}$ is the hydrogen production capacity range of the hydrogen production device; $C_{PceilN,1\sim4}$ is the hydrogen consumption capacity range of the fuel cell device; $C_{ccsN,1\sim4}$ is the capacity range of hydrogen storage equipment; $L_{c,1\sim4}$ is the corresponding access node number. The wind power output and photovoltaic output are taken as the predicted values and their upper and lower limits, respectively, to form four groups of uncertain scenarios. The installed capacity of the hydrogen production and storage system is determined by the upper optimization. In order to reflect the characteristics of the time period, the flexible load achieves peak-valley reduction and power balance through hydrogen production in trough and hydrogen release in peak.

According to the proportion of the cost of each part of the whole life cycle, table 1 gives the cost and electricity price data used in the example.

The construction cost of the hydrogen storage device in the system is about 34500 yuan/kg, the operation and maintenance cost is about 169 yuan/(kg·year), and the disposal cost is about 7000 yuan/kg. The Power purchase price is 0.3 yuan/(kW·h) and the hydrogen sales revenue is 7.8 yuan/m^3 during the grid trough period.

Table 1. Cost and electricity price data

Project type	Construction cost/ (Yuan·kW)	Operation and maintenance costs / (Yuan·kW·year)	Disposal cost / (Yuan·kW)	On-grid electricity price / (Yuan·kW·h)
wind power	7200	325	510	0.56
photovoltaic	9100	355	2300	0.63
Hydrogen production	6300	232	630	
Fuel Battery	3000	131	200·	0.64

4.2. System power balance and power flow optimization results

Figure 3 shows the time series distribution of each energy flow in the optimization stage, including power purchase P_{buy}, power sale P_{sell}, wind power, photovoltaic power, hydrogen production power P_{Zh2} and fuel cell discharge power P_{ceil}.

The output of various types of power in the optimization stage is shown. It can be seen that the load presents typical intra-day fluctuation characteristics, the photovoltaic reaches the peak during the day, and the wind power fluctuates randomly throughout the day. The P2G hydrogen production device improves the hydrogen production power during the period of high renewable energy output, and effectively absorbs excess electric energy. The fuel cell discharges moderately during the photovoltaic trough and peak load periods to compensate. On the whole, wind, solar, hydrogen production, hydrogen storage and fuel cells form a coordinated multi-energy complementary relationship, which improves the utilization rate of renewable energy and improves the balance of system operation.

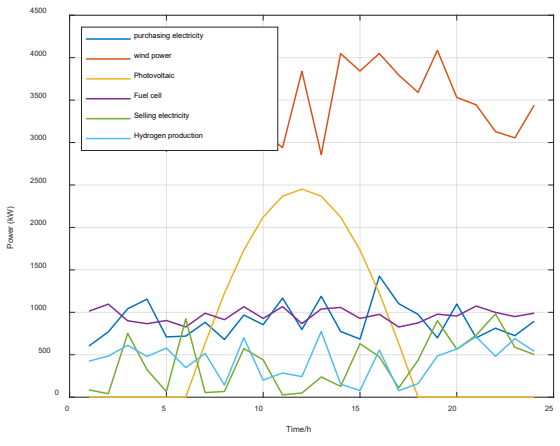

Figure 3. The optimal strategy diagram of the optimization stage

4.3. Analysis of wind and solar output consumption and prediction deviation

Figure 4 shows the comparison between the predicted power and the actual power of the four wind farms within 24 hours on a typical day. It can be seen that the predicted power curves of the four wind farms can well reflect the overall trend of the actual output, and the peak and valley periods of the output are highly consistent, indicating that the prediction model captures the timing characteristics of wind power more accurately. Each wind farm shows the characteristics of fluctuation with the change of wind speed in the whole day. The predicted value is close to the actual value, which fully reflects the randomness and dynamics of wind power change. In general, the prediction results of the four wind farms have good reference value, which provides a reliable basis for the system optimization scheduling and the subsequent wind-solar-hydrogen coordinated operation strategy.

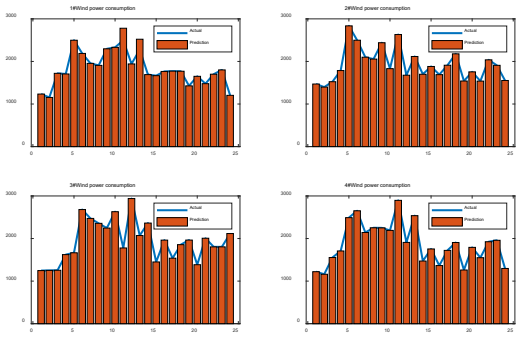

Figure 4. Comparison diagram of wind power output

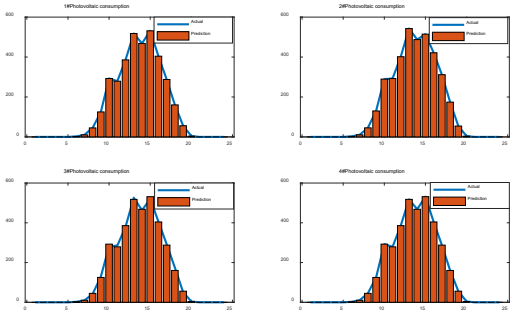

Figure 5. Comparison diagram of each photovoltaic electric field power

Figure 5 shows the comparison between the predicted irradiance and the actual irradiance of the four photovoltaic stations within 24 hours of a typical day. It can be seen that the irradiance of each station shows typical sunshine variation characteristics: gradually increasing in the morning, peaking at noon, and then decreasing rapidly in the evening. The predicted curve and the actual curve maintain a high consistency in the overall shape, and the peak time period and the change trend are in good agreement, which can effectively reflect the natural characteristics of irradiance changing with time. The results show that the photovoltaic irradiance prediction model has a good performance in capturing the variation law of all-day irradiation, which provides a reliable data basis for subsequent photovoltaic power prediction and integrated energy scheduling.

4.4. Peak-valley difference improvement effect

After the flexible hydrogen production and storage load is connected, the system load curve is smooth and obvious, the peak-valley difference is reduced from the original 41.2% to 23.6%, and the improvement rate is 42.7%.

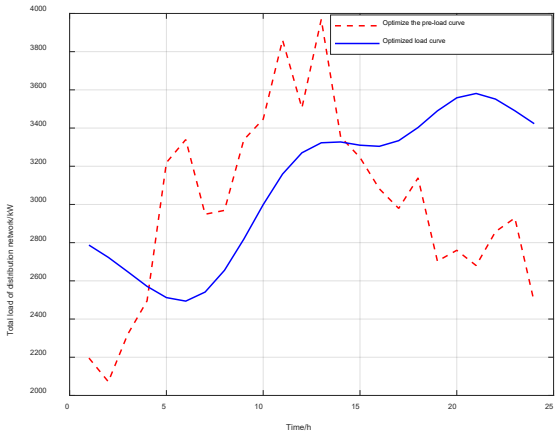

Figure 6. Peak-valley difference comparison diagram of total load curve of distribution network

Figure 6 illustrates the variations in the total load of the distribution network before and after optimization. Before optimization, the load curve fluctuates significantly, and there is an obvious peak-valley difference. After optimization, with the adjustment of flexible loads such as hydrogen production and hydrogen storage, the system load shows a smoother change trend, the peak-valley fluctuation is obviously converged, and the load curve is more flexible. The results show that the optimization model can effectively reduce the load pressure of the distribution network and improve the schedulability and predictability of the load curve.

4.5. Voltage distribution and line current carrying rate improvement effect

Figure 7 shows that the overall operational performance of the system is significantly improved after the integration of the flexible hydrogen production and storage load into the distribution network. The voltage of the terminal node (node 28-33) is obviously raised, and the minimum voltage is

increased from 0.913 *p.u* before access to 0.952 *p.u*, which effectively avoids the risk of low voltage. At the same time, the voltage distribution of the whole network is smoother, the voltage deviation level is further reduced, and the voltage difference between nodes is significantly reduced.

As shown in Figure 8, from the variation in the branch current carrying rate, the load of high current carrying rate branch decreases obviously, the maximum current carrying rate decreases from 90.3 % to 71.4 %, and the safety margin is significantly improved. The current carrying rate of most branches shows different degrees of decline, especially the branches that are close to the thermal limit. The current carrying rate is kept in a lower range, and the system security is significantly enhanced.

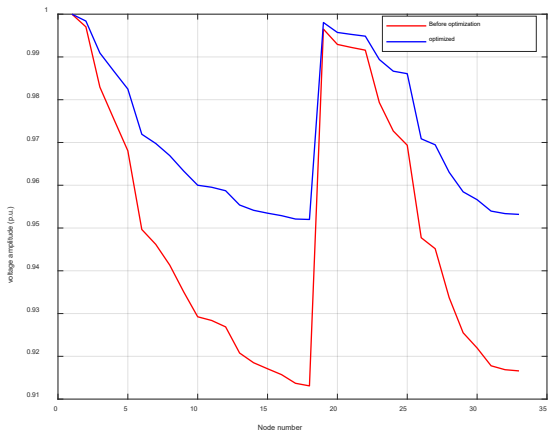

Figure 7. Node voltage distribution comparison diagram

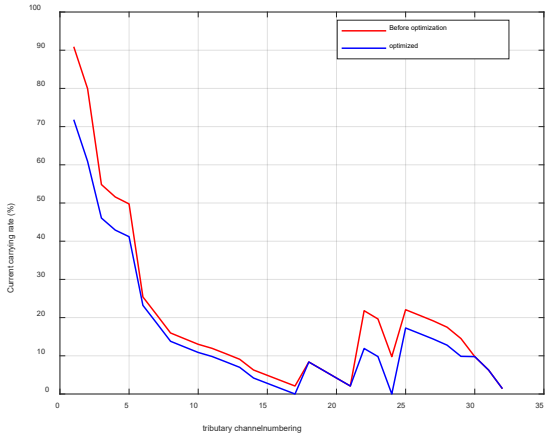

Figure 8. Comparison diagram of branch current-carrying rate distribution

The access of the flexible hydrogen production-storage unit can effectively absorb the fluctuating wind-solar power supply, and form a support in the low-voltage weak area to improve the voltage quality. The operating pressure of the high-load branch is reduced by peak shaving and valley filling, so as to significantly improve the operating state of the distribution network without additional line investment.

5. Conclusion

In this paper, a two-layer optimization method for wind-solar-hydrogen coupling system is proposed to solve the problems of large voltage fluctuation, uneven power flow distribution and high current carrying rate of distribution network under the background of high proportion of wind-solar access. The upper layer takes the capacity and access location of hydrogen production, hydrogen storage and fuel cell as decision variables, and constructs a life cycle cost model to realize the optimal planning of flexible load. The lower layer is based on YALMIP to construct a day-ahead operation optimization model. By optimizing wind and solar power generation, hydrogen production power, hydrogen storage status and fuel cell output, the system operation cost and operation risk are minimized. The simulation results show that the introduction of flexible hydrogen energy load significantly improves the operation state of the distribution network: the minimum voltage of the terminal node increases from 0.913 to 0.952, the maximum current carrying rate of the branch decreases from 90.3 % to 71.4 %, the load peak-valley difference decreases by 42.7 %, the system network loss is significantly reduced, and the renewable energy consumption capacity is effectively improved. The results verify the effectiveness of the bi-level optimization framework in the collaborative design of capacity configuration and operation scheduling. Future work can further consider wind and solar prediction errors, hydrogen production cost fluctuations, and equipment life models to enhance the applicability of the method in complex scenarios.

References

[1] Wen C, Xue F, Yang N, et al. Dual-level optimization model based on CNN-SWA prediction for smoothing wind-solar hydrogen production power fluctuation[J]. Energy Reports, 2025, 14: 3437-3450.

[2] Bagheri A, Monsef H, Lesani H. Integrated distribution network expansion planning incorporating distributed generation considering uncertainties, reliability, and operational conditions[J]. International Journal of Electrical Power & Energy Systems, 2015, 73: 56-70.

[3] Geng Q, Wang H, Wang S, et al. Reactive power and power flow optimization strategy of power system based on renewable energy access[J]. Microchemical Journal, 2025: 115833.

[4] Saeed M H, Fangzong W, Kalwar B A, et al. A review on microgrids' challenges & perspectives[J]. IEEe Access, 2021, 9: 166502-166517.

[5] Shafiullah G M, Oo A M T, Ali A B M S, et al. Potential challenges of integrating large-scale wind energy into the power grid–A review[J]. Renewable and sustainable energy reviews, 2013, 20: 306-321.

[6] Chen X, Dall'Anese E, Zhao C, et al. Aggregate power flexibility in unbalanced distribution systems[J]. IEEE Transactions on Smart Grid, 2019, 11(1): 258-269.

[7] Wang J, Wen J, Wang J, et al. Coordinated scheduling of wind-solar-hydrogen-battery storage system for techno-economic-

environmental optimization of hydrogen production[J]. Energy Conversion and Management, 2024, 314: 118695.
[8] Geng Y, Liu Q, Zheng H, et al. Two-Stage Collaborative Power Optimization for Off-Grid Wind–Solar Hydrogen Production Systems Considering Reserved Energy of Storage[J]. Energies, 2025, 18(11): 2970.
[9] Ma S, Mei S, Yu L. Research on multi-timescale operation optimization of a distributed electro-hydrogen coupling system considering grid interaction[J]. Frontiers in Energy Research, 2023, 11: 1251231.
[10] Meng Z, He Q, Shi X, et al. Research on energy utilization of wind-hydrogen coupled energy storage power generation system[J]. Separation and Purification Technology, 2023, 313: 123439.
[11] Niu M, Li X, Sun C, et al. Operation optimization of wind/battery storage/alkaline electrolyzer system considering dynamic hydrogen production efficiency[J]. Energies, 2023, 16(17): 6132.
[12] Yang Y, Xu X, Luo Y, et al. Distributionally robust planning method for expressway hydrogen refueling station powered by a wind-PV system[J]. Renewable Energy, 2024, 225: 120210.
[13] Mose M P, Kannaiyan S, Huang S J. Hydrogen Carriers for Hydrogen Transport and Storage (Hydrogen Storage): A Review[J]. Materials Chemistry and Physics, 2025: 131252.
[14] Mustapha H, Petrone R, Hammou A, et al. Sizing Optimization of a Grid-Connected System Considering Hydrogen Production Using Particle Swarm Optimization[C]//2025 International Conference on Control, Automation and Diagnosis (ICCAD). IEEE, 2025: 1-6.
[15] Nguyen T A, Kien L C, Duong M Q, et al. Total Fuel Cost, Power Loss, and Voltage Deviation Reduction for Power Systems with Optimal Placement and Operation of FACTS and Renewable Power Sources[J]. Applied Sciences, 2025, 15(19): 10596.
[16] Zhu G, Gao Y, Sun H. Optimal configuration of a wind-photovoltaic-hydrogen-gas-electric vehicles integrated energy system considering multiple uncertainties and carbon reduction[J]. Scientia Iranica, 2025, 32(1).
[17] Wang H, Chen X, Yang Q, et al. Optimization of renewable energy hydrogen production systems using volatility improved multi-objective particle swarm algorithm[J]. Energies, 2024, 17(10): 2384.
[18] Abdalla A M, Hossain S, Nisfindy O B, et al. Hydrogen production, storage, transportation and key challenges with applications: A review[J]. Energy conversion and management, 2018, 165: 602-627.
[19] Ma Y, Hu Z, Song Y. Stability-Guaranteed Optimization of Adaptive Primary and Secondary Frequency Control Strategies Considering Flexible Resources[J]. IEEE Transactions on Power Systems, 2025.
[20] Yan Q, Zhang G, Zhang Y, et al. Coordinated scheduling optimization of building integrated energy system with flexible load[J]. Energy Reports, 2024, 12: 3422-3436.
[21] Sun D, Yu J, Zheng W, et al. Multi-energy cooperative primary frequency regulation analysis of a hybrid plant station for wind power and hydrogen production based on ensemble empirical-mode decomposition algorithm[J]. Applied Sciences, 2023, 13(22): 12394.
[22] Pengfei L. Study on capacity optimal configuration and energy management of integrated wind-solar-hydrogen-storage power supply system[J]. Zhe Jiang University, 2017.
[23] Jimin Z. Performance simulation and energy management of hybrid wind-pemfc power generation system[D]. Ph. D. dissertation, Dept. Elect. Eng., Shandong University, 2017.
[24] Chengzhen J I A, Lingmei W, Enlong M, et al. Optimal capacity configuration and day-ahead scheduling of wind-solar-hydrogen coupled power generation system[J]. Electric Power, 2020, 53(10): 80.
[25] Pu Y, Li Q, Chen W R, et al. Energy management for islanded DC microgrid with hybrid electric-hydrogen energy storage system based on minimum utilization cost and energy storage state balance[J]. Power Syst. Technol, 2019, 43(03): 918-927.